

# Relativistic magnetospheres of rotating cosmic objects – the regime of force–free surfaces

P. Biltzinger and K.O. Thielheim\*

\* University Kiel, Department of Physics, 24118 Kiel, Germany

**Abstract.** Selfconsistent magnetospheres of rotating cosmic magnets with arbitrary inclination of the magnetic against the rotational axis are considered. Present studies concentrate on the regime dominated by the force–free surface (FFS). A classical macroscopic fluid description is applied and radiation reaction is taken into account. As in earlier work of our group, a 'standard set of parameters' is used. Under these conditions, the following features are found among other results: global charge separation exists for all degrees of inclination of the magnetic against the rotational axis; clouds of different charge are separated by regions of vanishing particle number density; as expected, test particles inserted into the latter regions propagate into one of the adjacent clouds. Strong poloidal currents exist; locally averaged particle energies typically range up to  $10^{16} - 10^{17}$  eV, depending on the angle of inclination.

PACS numbers: 52.25.Wz Nonneutral Plasmas, 52.60.+h Relativistic plasma, 52.65.-y Plasma simulation, 98.70.Sa Cosmic rays, 97.60.Jd Neutron stars

## 1. Introduction

Since the discovery of pulsars in 1968 [1] and their interpretation as a rapidly rotating magnetized neutron stars in the same year [2, 3], these compact objects are under discussion as powerful accelerators of ultra high energy cosmic ray particles.

From the very beginning of neutron star physics, work on the dynamics of electrically charged particles accelerated in the corresponding electromagnetic fields proceeded on two stages: (1) test particle dynamics in the vacuum fields of rotating magnets, e.g. [4, 5], demonstrating fundamental mechanisms and (2) self consistent plasma dynamics, e.g. [6], reproducing certain aspects of the structure and evolution of neutron star magnetospheres.

Since then, numerous papers have been published, investigating these matters in great detail, which we will not be able to discuss or even just to mention in this introduction to our present paper. Here, we shall concentrate, on stage (2), on relativistic plasma dynamics in a regime governed by the force–free surface of a homogeneously magnetized, rapidly rotating sphere, with parameters typical for neutron stars.

The notation of a force–free surface (FFS) refers to the dynamic of an electrically charged (test) particle within given electromagnetic fields. By definition the FFS is

generated by those points of configuration space at which the Lorentz–force acting on that particle through given electromagnetic fields vanishes. While in published literature a particle that happens to be at such a point often referred to as 'force-free' (ff), we prefer – in view of the presence of other types of electromagnetic forces (radiation reaction forces) – to speak of a Lorentz–force–free (Lff) particle in that situation. If‡  $\mathbf{B} \neq 0$  and  $\mathbf{E} \neq 0$ , as is the case in fields considered here, a particle is Lff for  $\mathbf{E} + [\boldsymbol{\beta}, \mathbf{B}] = 0$ , i.e., for (I)  $(\mathbf{E}, \mathbf{B}) = \mathbf{0}$  and (II)  $(\mathbf{E}, \boldsymbol{\beta}) = \mathbf{0}$  and (III)  $([\mathbf{E}, \mathbf{H}], \boldsymbol{\beta}) = |\mathbf{E}^2|$ .  $\mathbf{E}$  is the electric field vector,  $\mathbf{B}$  the vector of the magnetic induction and  $\boldsymbol{\beta}$  is the velocity in units of the velocity of light. For  $|\mathbf{E}| \ll |\mathbf{B}|$ , as is the case under premises adopted here, one may expect the second and the third conditions to be inherently fulfilled to some approximation so that the FFS then is characterized solely by the first condition,  $(\mathbf{E}, \mathbf{B}) = \mathbf{0}$ .

From the early works of [7, 8], magnets rotating in the vacuum with the vector of magnetic dipole moment inclined against their respective rotational axis, are known to create such FFS, of which some segments can act as particle traps and thus may have strong bearings on the formation of a neutron star magnetosphere, at least within a certain range of distance from its surface.

In what follows, it will be useful to distinguish the special case of *aligned rotators*, i.e. rotating magnets with the magnetic axis parallel to the rotational axis (*parallel rotators*) or antiparallel to the rotational axis (*antiparallel rotators*), from the general case of *inclined rotators* and from rotating magnets with the magnetic axis orthogonal to the rotational axis (*orthogonal rotators*). On stage (2), a considerable number of investigations has been published on aligned rotators. Some of these papers will be mentioned below. But only few are devoted to inclined or orthogonal rotators. In the latter case, obviously, considerable formal and numerical complications arise from the lack of rotational symmetry. Analytical approaches were used, for example, by [8, 9, 10, 11].

In the special case of aligned rotators, due to axial symmetry, theoretical results are achieved much easier, even on stage (2). Analytical methods, for example, have been applied to the structure of the magnetosphere of aligned rotators by [6, 7, 12, 13, 14, 15, 16, 17, 18]. Also, numerical studies on that matter have been performed by [19, 20, 21, 22, 23, 24].

On stage (1) in an earlier work of our group [25] the authors have integrated numerically the equation of motion for individual test particles, within the regime of the FFS and with no restrictions on the relative orientation of the rotational towards the magnetic axis. Results confirm that velocity components orthogonal to the magnetic field vector are efficiently damped by radiation reaction. Thus, test particles tend to follow magnetic field lines, as suggested earlier by [7]. In a certain class of orbits, they oscillate about the FFS, while moving along magnetic field lines. The amplitude of these oscillations decreases through radiation losses. Ultimately, in the subsequent regime of

‡ Boldface letters are for vectors in 3-dimensional euclidean space.  $(\cdot, \cdot)$  denotes the scalar product,  $[\cdot, \cdot]$  the vector product.

(lower) energy (and on a much larger time scale,) particles become subject to drift in azimuthal direction.

On stage (2) in a second paper of our group [26] the authors have introduced a numerical iterative approach to reproduce sequences of quasi stable plasma configurations forming under the influence of the FFS. In iterative steps, charged particles were allowed to be ejected from surface elements of the rotating sphere in quantities locally proportional to the magnitude of the electric vector component normal to the respective surface element. These particles were then allowed to move freely along the appropriate magnetic field lines and to settle down where the projection of the electric onto the magnetic vector vanishes. Thus, *without making use of the equation of motion*, co-rotating, quasi stable, charge separated clouds were reproduced, in consistency with earlier results mentioned above.

In our present work, we proceed one step further taking into account in a selfconsistent way virtually *all effects of relativistic particle dynamics*, including radiation reaction and effects of special relativity as, for example, retardation. Our numerical approach is designed to describe the evolution of locally averaged particle densities, since velocity dispersion is not taken into account. Again, a magnetosphere is allowed to build up from the initial vacuum through particle ejection from the spherical surface, similar to the procedure described above<sup>§</sup>.

Thereby, we intend to clarify, on stage (2), the evolution, selfconsistent structure and stability properties of plasma configurations forming within the regime of the FFS of a rotating cosmic magnet with no restrictions on the relative orientation of the rotational towards the magnetic axis. Also, we want to evaluate mean energy values locally achieved by particles in that regime.

As in earlier works of our group, e.g. [27, 28, 29], we shall apply a model represented by a rotating, ideally conducting, homogeneously magnetized sphere with arbitrary inclination of the magnetic against the rotational axis. A 'standard set of parameters' representing well-known properties of typical neutron stars is attributed to this model: the stellar mass which is taken equal to the solar mass,  $m_N = m_{\text{sun}}$ , the stellar radius,  $r_N = 10^6 \text{ cm}$ , the angular velocity,  $\omega = 20 \pi \text{ s}^{-1}$ , and the magnetic dipole moment<sup>||</sup>  $\mu = 10^{30} \text{ G cm}^3$ . Also, we shall concentrate on the near zone of electromagnetic fields of the inclined rotator, up to about  $20 r_N$ .

From preceeding estimates as well as from subsequent simulations gravitational forces exerted by the rotating neutron star and by the magnetosphere itself onto

<sup>§</sup> Here, particles are allowed to be ejected from surface elements, (given an appropriate direction of the electric vector,) in quantities locally proportional to the magnitude of the electric vector component projected onto the magnetic field line.

<sup>||</sup> Gaussian units are used throughout this paper. Thus, electric and magnetic field strengths are measured in units of  $1 \text{ G} = 300 \text{ V/cm}$ . For the standard set of parameters, the magnetic field strength is about  $B_p \simeq 2 \cdot 10^{12} \text{ G}$  and the electric field strength is approximately  $E_p \simeq 10^{10} \text{ G}$  in the polar region. Under given parameter values, the radius of the light-cylinder, (often referred to as 'light radius')  $r_L = \omega / c$ , outside of which corotation cannot exist, is  $r_L = 5000 \text{ km}$ , corresponding to almost the radius of the earth, for comparison.

individual particles, as well as effects of general relativity were found to be negligible for the standard set of parameters. Contributions to the Lorentz–force originating from magnetic fields created by magnetospheric particle currents can also be neglected, in agreement with earlier conclusions of [22]. Spontaneous pair creation still turns out to be insignificant, even within the very strong electromagnetic fields of polar regions.

Computations described in this paper have greatly profited from (yet unpublished) simulation software, developped by H. Laue, K.O. Thielheim and other members of the Mathematical Physics Devision of the former Institut für Kernphysik of Kiel University. This software, which we refer to as 'emp' (for electromagnetic particles), was made for N-body simulations of neutron star magnetospheres under premises identical to those adopted here.

In chapter 2 of what follows, we shall rediscuss vacuum fields and force–free surfaces associated with rotating magnets. Thereafter, in chapter 3, we shall display equations of *individual* as well as of *collective particle motion* in terms of a non-neutral two-component fluid, and we shall then proceed to a description of appropriate tools for numerical treatment in chapter 4. Results will be given in chapter 5 and subsequently discussed there.

## 2. Vacuum Fields and Force–Free Surfaces

The vacuum solution of Maxwell's equations for a homogeneously magnetized (ideally conducting) sphere, rotating with its vector of angular velocity  $\boldsymbol{\omega}$  inclined relative to its vector of magnetic dipol moment  $\boldsymbol{\mu}$  by the angle  $\chi$ , as evaluated in [30], called Deutsch–field, may be applied here in the near–field approximation. In addition, to account for the global electric charge of the rotating sphere, an electric monopol contribution  $q_s$  is introduced:

$$\begin{aligned} B_r(\mathbf{r}, t) &= 2 \frac{\mu}{r^3} (\cos \chi \cos \vartheta + \sin \chi \sin \vartheta \cos \lambda), \\ B_\vartheta(\mathbf{r}, t) &= \frac{\mu}{r^3} (\cos \chi \sin \vartheta - \sin \chi \cos \vartheta \cos \lambda), \\ B_\varphi(\mathbf{r}, t) &= \frac{\mu}{r^3} \sin \chi \sin \lambda, \\ E_r(\mathbf{r}, t) &= \frac{q_s}{r^2} - \frac{1}{2} \frac{\mu}{r_L} \frac{r_N^2}{r^4} [\cos \chi (3 \cos 2\vartheta + 1) + 3 \sin \chi \sin 2\vartheta \cos \lambda], \\ E_\vartheta(\mathbf{r}, t) &= - \frac{\mu}{r_L} \frac{r_N^2}{r^4} [\cos \chi \sin 2\vartheta + \sin \chi \cos \lambda [(r/r_N)^2 - \cos 2\vartheta]], \\ E_\varphi(\mathbf{r}, t) &= \frac{\mu}{r_L} \frac{r_N^2}{r^4} [(r/r_N)^2 - 1] \sin \chi \cos \vartheta \sin \lambda. \end{aligned} \quad (1)$$

Here, we make use of two sets of spherical coordinates: one is referred to as the  $\omega$ –system  $(r, \vartheta, \varphi)$ , where  $r$  is the radial coordinate,  $\vartheta$  is the angle measured against the rotational axis, and  $\varphi$  is the angle relative to the plane spanned by the  $\mathbf{x}_0$  and  $\mathbf{y}_0$  axes, at rest in a chosen inertial frame of reference.

The other set of spherical coordinates is referred to as the  $\mu$ –system  $(r, \psi, \lambda)$ , in

which  $\psi$  is the angle relative to the magnetic dipol axis, and  $\lambda$  is the angle against the plane spanned by the  $\mu$  and  $\omega$  axes. As a consequence of these definitions,  $\lambda = \varphi - \omega[t - (r - r_N)/c]$ . Both coordinate systems are illustrated by figure 1.

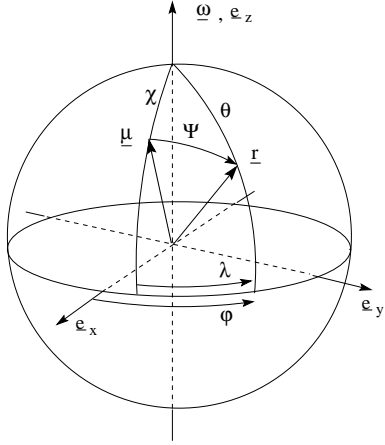


**Figure 1.** Coordinates

In the case of an ideally conducting sphere, the topography of the exterior field is known to be independent of the form of interior magnetization. An interior central magnetic point dipole, which may be chosen as an alternative model of magnetization, obviously would create the same electromagnetic vacuum field configuration. But the electric surface charge as well as the interior charge evoked by rotation clearly depend on the form of magnetization.

A central interior magnetic point dipole, for example, is consistent with the total interior electric charge  $Q_i = \frac{2}{3} \frac{\mu}{r_L} \cos \chi$  and with the surface charge density

$$\sigma = -\frac{\mu}{2\pi r_L r_N^2} [\cos \chi \cos^2 \vartheta + \sin \chi \cos \theta \sin \vartheta \cos(\varphi - \omega t)] \quad (2)$$

corresponding to the total surface charge  $Q_s = -\frac{2\mu}{3r_L} \cos \chi$ . Alternatively, for a homogeneously magnetized sphere, as considered throughout this paper, the surface charge density is

$$\sigma = -\frac{\mu}{4\pi r_L r_N^2} [\cos \chi (5 \cos^2 \vartheta - 3) + 5 \sin \chi \cos \vartheta \sin \vartheta \cos(\varphi - \omega t)] \quad (3)$$

and  $Q_i = \frac{4\mu}{3r_L} \cos \chi = -Q_s$ .

The discontinuity of the tangential component of the magnetic surface field creates an electric surface current which results negligible under conditions given here.

With the projection of the electric onto the magnetic vector, written in the  $\mu$ -system,

$$\begin{aligned} \frac{(\mathbf{E}, \mathbf{B})}{B} = & -\frac{\mu k^3}{(k r)^4} \frac{1}{\sqrt{1 + 3 \cos^2 \psi}} \left[ (r/r_N)^2 (\sin \chi \sin \psi \cos \lambda - 2 q'_s \cos \psi) \right. \\ & \left. + 4(\cos \chi \cos \psi - \sin \chi \sin \psi \cos \lambda) \cos^2 \psi - \sin \chi \sin \psi \cos \lambda \right] \quad (4) \end{aligned}$$

the FFS is given by

$$\left(\frac{r}{r_N}\right)^2 = \frac{(\sin \chi \sin \psi \cos \lambda - 4(\cos \chi \cos \psi \sin \chi \cos \lambda \sin \psi) \cos^2 \psi)}{(\sin \chi \sin \psi \cos \lambda - 2q'_s \cos \psi)}, \quad (5)$$

where  $q'_s := q_s \frac{r_L}{\mu}$  is the dimensionless form of the total electric charge of the sphere.

This formal expression is further illustrated by figures 2–3.

### 3. Non–Neutral Two–Component Plasma Fluid

#### 3.1. Equations of Motion for the Plasma

We consider a classical two–component ideal fluid, each component of which (identified by the index  $s = 1, 2$ ) consists of  $N$  identical (classical) particles, electrons and protons in this case. For a relativistic macroscopic description of fluid motion in terms of the one–particle distribution function  $\mathcal{F}_s(x^\mu, p^\mu)$ , we start with the one–particle Liouville–equation

$$\frac{d\mathcal{F}_s}{d\tau} = \dot{x}^\mu \frac{\partial \mathcal{F}_s}{\partial x^\mu} + \dot{p}^\mu \frac{\partial \mathcal{F}_s}{\partial p^\mu} = 0, \quad (6)$$

where  $x^0 = ct$  is the time coordinate,  $x^i$  are the spatial coordinates,  $p^\mu$  are the four corresponding components of momentum<sup>¶</sup>. Using the covariant form of Hamilton’s equations,  $dx^\mu/d\tau = \partial \mathcal{H}/\partial p_\mu$  and  $dp^\mu/d\tau = -\partial \mathcal{H}/\partial x_\mu$ , where  $\mathcal{H}$  is the Hamilton–function, one may write the covariant Vlasov–equation in the form

$$\frac{\partial}{\partial x^\mu}(\mathcal{F}_s \dot{x}^\mu) + \frac{\partial}{\partial p^\mu}(\mathcal{F}_s \dot{p}^\mu) = 0. \quad (7)$$

With the definition of the one–particle distribution function<sup>+</sup>

$$f_s(x^\mu, p^k) := \int_{-\infty}^{\infty} \mathcal{F}_s(x^\mu, p^\nu) dp^0, \quad (8)$$

the Vlasov–equation results in <sup>\*</sup>

$$\frac{\partial}{\partial x^\mu}(f_s \dot{x}^\mu) + \frac{\partial}{\partial p^i}(f_s \dot{p}^i) = 0. \quad (9)$$

If  $u^\mu = dx^\mu/d\tau$  are the four components of velocity,  $a^\mu = du^\mu/d\tau$  those of the acceleration, while  $\gamma$  is the Lorentz–factor and  $\tau$  the proper time, the Vlasov–equation can be represented by

$$\frac{\partial}{\partial t}(\gamma f_s) + c \frac{\partial}{\partial x^i}(u^i f_s) + \frac{\partial}{\partial u^i}(a^i f_s) = 0. \quad (10)$$

The distribution function  $f_s(x^\mu, u^i)$  by integration delivers namely

$$n_s(x^\mu) = \int f_s(x^\mu, u^i) d^3 u \quad (11)$$

¶ The signature of the metric tensor is (1,-1,-1,-1). Throughout this paper, Greek indices are running from 0 to 3, latin indices from 1 to 3. As stated before, effects of general relativity (including gravitation) are left unaccounted for since, with the standard set of parameters, the Schwarzschild–radius is only about  $r_s \approx 0.3 r_N$ .

<sup>+</sup>  $f_s(x^\mu, p^k)$  is a scalar under Lorentz–transformations.

<sup>\*</sup> With the assumption  $\mathcal{F} \rightarrow 0$  for  $p^\mu \rightarrow \infty$ .

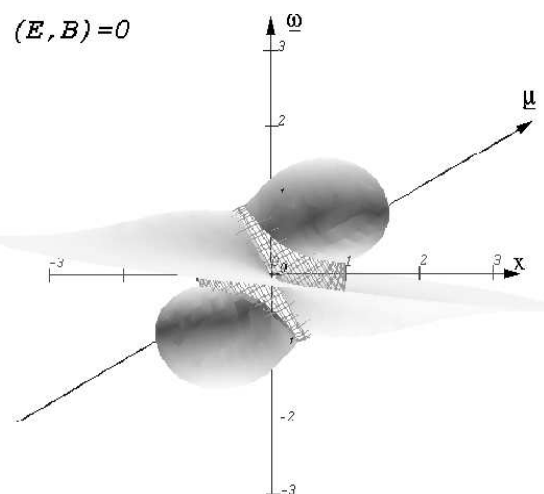
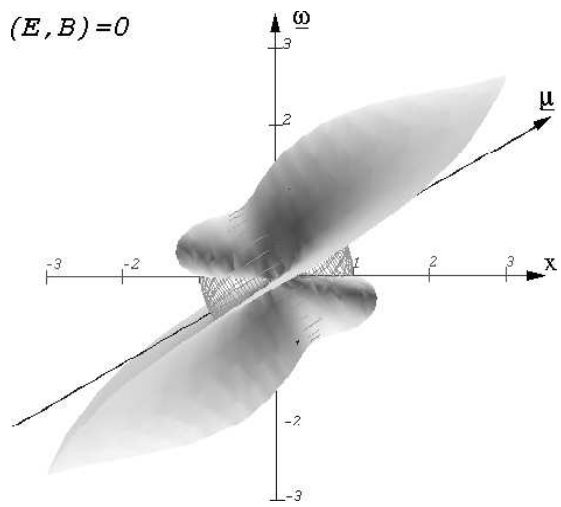


**Figure 2.**  $\chi = 60^\circ$ : Force-Free Surface. The right sphere is electrical uncharged and the left sphere has an additional electrical charge  $q_s = 0.3 \mu/r_L$ . The unit of length on both axes is  $r_N$ .

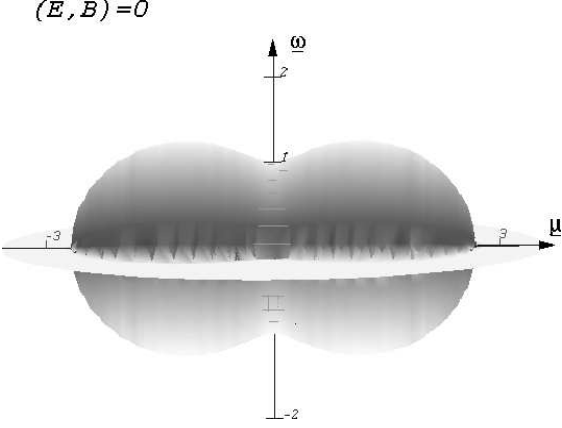


**Figure 3.**  $\chi = 90^\circ$ : Force-Free Surface. The sphere is electrical uncharged in this example. Again, the unit of length on both, the ordinate and the abscissa, is  $r_N$ .

and from there the average, macroscopic (four-component) velocity vector

$$\bar{u}_s^\mu(x^\mu) = n_s^{-1} \int u^\mu f_s(x^\mu, u^i) d^3u \quad (12)$$

and the electric charge density

$$\varrho(x^\mu) = \sum_s e_s n_s(x^\mu). \quad (13)$$

Likewise, we make use of the average, macroscopic (three-component) velocity vector  $\bar{v}_s^i(x^\mu)$  to define the electric current density

$$j^i(x^\mu) = \sum_s e_s \int v^i f_s d^3u = \sum_s e_s \bar{v}_s^i(x^\mu) \quad (14)$$

constituting thereby the four components of the electric current density vector field  $j^\mu = (c\varrho, j^i)$ .

The latter, in consistency with (10), act as source terms in Maxwell's equations

$$\partial_\alpha F^{\alpha\beta} = \frac{4\pi}{c} j^\beta, \quad \partial_\alpha F^{\star\alpha\beta} = 0, \quad (15)$$

where  $F^{\alpha\beta} = \partial^\alpha A^\beta - \partial^\beta A^\alpha$  is the electromagnetic field tensor and  $F^{\star\alpha\beta} = \frac{1}{2}\epsilon^{\alpha\beta\gamma\delta} F_{\gamma\delta}$  its dual counterpart.  $A^\mu$  is the electromagnetic potential.  $\epsilon^{\alpha\beta\gamma\delta}$  is the Levi-Civita-tensor.

The average number density  $n_s(x^\mu)$  and velocity  $\bar{u}_s^i(x^\mu)$  fields of each of the two constituents of the plasma serve to describe macroscopic fluid motion with the help of the continuity equation

$$\frac{\partial n_s}{\partial t} + \frac{\partial}{\partial x^i} (n_s \bar{v}_s^i) = - \int \frac{\partial}{\partial u^i} (a^i f_s) d^3u = 0, \quad (16)$$

obtained from (10) through integration over velocity space, adopting  $|\mathbf{a}|f_s \rightarrow 0$  for  $|\mathbf{u}| \rightarrow \infty$ . As is well known, the energy-momentum equation

$$\frac{\partial \bar{u}_s^i}{\partial t} + \bar{v}_s^j \frac{\partial}{\partial x^j} \bar{u}_s^i = \frac{1}{(m_s n_s)} \left( -\partial_j p_s^{ij} + \mathcal{K}^i \right), \quad (17)$$

is obtained from (10) through multiplication with  $u^j$  and integration over the velocity space, where

$$p_s^{ij}(x^\mu) = \int m_s(u^i - \bar{u}_s^i)(u^j - \bar{u}_s^j) f_s d^3 u = m_s \int u^i u^j f_s d^3 u - m_s n_s \bar{u}_s^i \bar{u}_s^j \quad (18)$$

is the pressure tensor and  $m_s$  is the rest mass of particles constituting the respective plasma component.

In what follows, we shall adopt the notion of a collisionless, dispersionless (i.e. 'cold'), relativistic plasma†. Thus, the right side of equation (17) reduces to the (volume) force term

$$\mathcal{K}^i = m_s \int a^i f_s d^3 u, \quad (19)$$

to which the Lorentz–force is expected to deliver a major contribution  $\mathcal{K}^\mu_{Lorentz} = \eta_0 F^{\mu\nu} \bar{u}_\nu$ , where  $\eta_0 = e/(mc)$ .

### 3.2. Equations of Motion for Individual Electrically Charged Particles

In addition to the Lorentz–force the classical equation of motion for an electrically charged *relativistic* particle subject to given ('external') electromagnetic fields has to account for radiation reaction forces. One such equation, which frequently is called 'Lorentz–Dirac (LD) equation' [31], (though Abraham–Lorentz (AL) equation would be historically more correct) may be given the form

$$\frac{du^\mu}{d\tau} = \eta_0 F^{\mu\nu} u_\nu + \tau_0 G^{\mu\nu} u_\nu \quad (20)$$

suggested by one of us [32]. Here,

$$G^{\mu\nu} = G_{LD}^{\mu\nu} = \frac{1}{c^2} (u^\nu \frac{d^2 u^\mu}{d\tau^2} - u^\mu \frac{d^2 u^\nu}{d\tau^2}) \quad (21)$$

is the radiation force tensor and  $\tau_0 = 2e^2/(3mc^3)$  is the radiation constant. Unfortunately, this equation of motion exhibits serious deficiencies which have extensively been discussed in published literature and can be avoided through replacement of (21) by its first iteration often referred to as 'Lorentz–Dirac–Landau (LDL) equation', (due to its extensive discussion in [33] well known textbook). In this approximation†, the radiation tensor may be written

$$G^{\mu\nu} = \eta_0 u_\lambda \partial^\lambda F^{\mu\nu} + \frac{1}{c^2} (u_{LL}^\mu u^\nu - u^\mu u_{LL}^\nu), \quad (22)$$

with  $u_{LL}^\mu = \eta_0^2 F^{\mu\nu} F_{\nu\lambda} u^\lambda$ . In our numerical work presented further below we shall adopt that *locally* (i.e. within appropriately small intervals of space and time coordinates,) the

‡ This assumption appears not implausible, since with a neutron star surface temperature of about  $10^5 - 10^7$  K and a particle density of about  $n_s \approx 10^{12} \text{ cm}^{-3}$  as suggested by the Goldreich & Julian–model (1969), the plasma parameter  $\Lambda = (4\pi/3)n_s \lambda_D^3$  results of the order of  $\Lambda \approx 10^7$  that is  $\Lambda \gg 1$ , where  $\lambda_D = \sqrt{k_B T/(4\pi n_s e^2)}$  is the Debye–length.

† One of us (Thielheim (1994)) has argued that in a quantum-mechanical frame self-consistency of classical electrodynamics suggests (22) to be the correct form of the radiadion tensor  $G^{\mu\nu}$ .

electromagnetic field is (approximately) homogenous in space and constant in time, in which case the radiation tensor (22) further reduces to

$$G^{\mu\nu} = G_{const}^{\mu\nu} = \tau_0 \eta_0^2 \left[ F_\nu^\alpha F_\lambda^\nu u^\lambda + F_\varrho^\lambda F_\lambda^\varphi u^\varrho u_\varphi u^\alpha \right]. \quad (23)$$

Under these premises, individual particles of each of the two plasma components, according to  $s = 1$  or  $2$ , inside the proper interval of space and time coordinates, (i.e. inside the corresponding 'volume element',) are subject to the *same* electromagnetic forces. Consequently, the (macroscopic field) equations for the plasma fluid‡ immediately follows from (17) and (20) with (23)

$$\bar{u}_{\beta,s} \partial^\beta \bar{u}_s^\alpha = \eta_0 F^{\alpha\beta} \bar{u}_{\beta,s} + \tau_0 \eta_0^2 \left[ F_\nu^\alpha F_\lambda^\nu \bar{u}_s^\lambda + F_\varrho^\lambda F_\lambda^\varphi \bar{u}_s^\varrho \bar{u}_{\varphi,s} \bar{u}_s^\alpha \right]. \quad (24)$$

### 3.3. Exact Solutions of the Equation of Motion for Individual Particles in Homogenous and Constant Fields

In what follows, we make use of exact analytical solutions of the equation of motion (23) for individual electrically charged particles in locally constant and homogenous electromagnetic fields (Thielheim, 1989). Given a coordinate system with  $\mathbf{e}_3 = \mathbf{B}$ ,  $\mathbf{e}_2 = [\mathbf{E}, \mathbf{B}]$  and  $\mathbf{e}_1 = [\mathbf{e}_2, \mathbf{e}_3]$ , and excluding null fields§ (i.e. fields with simultaneously vanishing Lorentz–invariants  $(\mathbf{E}, \mathbf{B})$  and  $\mathbf{E}^2 - \mathbf{B}^2$ ) and restricting further to  $E_1 \neq 0$  and  $B \neq 0$ , the solution of (23) is

$$u^\alpha(\tau) = \gamma a(\tau) \left\{ C_0 \begin{pmatrix} \cosh \lambda \tau \\ \beta \frac{\lambda}{\Omega_L} \sinh \lambda \tau \\ -\beta \cosh \lambda \tau \\ \frac{\omega}{\Omega_L} \sinh \lambda \tau \end{pmatrix} + C_3 \begin{pmatrix} \sinh \lambda \tau \\ \beta \frac{\lambda}{\Omega_L} \cosh \lambda \tau \\ -\beta \sinh \lambda \tau \\ \frac{\omega}{\Omega_L} \cosh \lambda \tau \end{pmatrix} \right\} \\ + \gamma b(\tau) \left\{ C_1 \begin{pmatrix} \beta \sin \omega \tau \\ \frac{\omega}{\Omega_L} \cos \omega \tau \\ -\sin \omega \tau \\ -\beta \frac{\lambda}{\Omega_L} \cos \omega \tau \end{pmatrix} + C_2 \begin{pmatrix} -\beta \cos \omega \tau \\ \frac{\omega}{\Omega_L} \sin \omega \tau \\ \cos \omega \tau \\ -\beta \frac{\lambda}{\Omega_L} \sin \omega \tau \end{pmatrix} \right\} \quad (25)$$

with

$$\lambda = \text{sign}(E_3) \frac{e}{mc} \sqrt{-\frac{1}{2}(B^2 - E^2) + \frac{1}{2}\sqrt{(B^2 - E^2)^2 + 4(\mathbf{E}, \mathbf{B})^2}}, \quad (26)$$

$$\omega = \frac{e}{mc} \sqrt{\frac{1}{2}(B^2 - E^2) + \frac{1}{2}\sqrt{(B^2 - E^2)^2 + 4(\mathbf{E}, \mathbf{B})^2}}, \quad (27)$$

$$\beta = \frac{E^2 + B^2 - \sqrt{(B^2 - E^2)^2 + 4(\mathbf{E}, \mathbf{B})^2}}{2 E_1 B}, \quad (28)$$

‡ Density effects on radiation and radiation reaction remain unaccounted for. Remarkably, since in (24) the pressure term is absent, the number density does not appear. Clearly, (24) governs the macroscopic velocity fields  $\bar{u}_s^\lambda$ .

§ Inside the magnetosphere,  $|\mathbf{E}| \ll |\mathbf{B}|$ .

$$\gamma = \frac{1}{\sqrt{2}} \sqrt{\frac{B^2 + E^2}{\sqrt{(B^2 - E^2)^2 + 4(\mathbf{E}, \mathbf{B})^2}} + 1}, \quad (29)$$

$$\Omega_L = \frac{e}{mc} B, \quad (30)$$

$$\begin{pmatrix} C_0 \\ C_1 \\ C_2 \\ C_3 \end{pmatrix} = \gamma \begin{pmatrix} u^0(0) + \beta u^2(0) \\ \frac{\omega}{\Omega_L} u^1(0) - \beta \frac{\lambda}{\Omega_L} u^3(0) \\ \beta u^0(0) + u^2(0) \\ \beta \frac{\lambda}{\Omega_L} u^1(0) + \frac{\omega}{\Omega_L} u^3(0) \end{pmatrix}$$

and the radiation parameters:

$$a(\tau) = [(C_0^2 - C_3^2) - (C_1^2 + C_2^2) \exp[-2\tau_0(\lambda^2 + \omega^2)\tau]]^{-\frac{1}{2}}, \quad (31)$$

$$b(\tau) = a(\tau) \exp[-\tau_0(\lambda^2 + \omega^2)\tau], \quad (32)$$

where  $C_\mu C^\mu = 1$ .

If the electric field is parallel (or antiparallel) to the magnetic one ( $E_1 = 0$ ), this solution reduces to:

$$u^\alpha(\tau) = a(\tau) \left\{ u^0(0) \begin{pmatrix} \cosh \lambda \tau \\ 0 \\ 0 \\ \sinh \lambda \tau \end{pmatrix} + u^1(0) \begin{pmatrix} 0 \\ \cos \omega \tau \\ -\sin \omega \tau \\ 0 \end{pmatrix} \right\} + b(\tau) \left\{ u^2(0) \begin{pmatrix} 0 \\ \sin \omega \tau \\ \cos \omega \tau \\ 0 \end{pmatrix} + u^3(0) \begin{pmatrix} \sinh \lambda \tau \\ 0 \\ 0 \\ \cosh \lambda \tau \end{pmatrix} \right\}. \quad (33)$$

The dynamics of a charged particle starting at rest is characterized by the following properties: Within a regime of small proper time,  $\tau \ll 1/\tau_0(\omega^2 + \lambda^2)$ , the radiation parameters are about  $a(\tau) \approx b(\tau) \approx 1$ , while particle motion is a composit of gyration around magnetic field lines,  $[\mathbf{E}, \mathbf{B}]$ -drift, and acceleration along magnetic field lines, due to the projection of the electric field vector onto to the tangent to the magnetic field line.

Within a regime of large proper time,  $\tau \rightarrow \infty$ , gyrations around magnetic field lines are damped corresponding to  $b(\tau) \rightarrow 0$ , while acceleration along magnetic field lines proceeds correspondig to  $a(\tau) \rightarrow 1$ , superimposed by  $[\mathbf{E}, \mathbf{B}]$ -drift and curvature drift.

In the magnetospherical regime considered here ( $|\mathbf{E}| \ll |\mathbf{B}|$ ), where  $\omega \approx \Omega_L, \lambda \approx \Omega_L \frac{E}{B} \sin \alpha$  and

$$\frac{1}{\tau_0(\omega^2 + \lambda^2)} \approx \begin{cases} 5 \cdot 10^{-16} \text{ s} & \text{for electrons} \\ 3 \cdot 10^{-6} \text{ s} & \text{for protons,} \end{cases} \quad (34)$$

gyrations around magnetic field lines are damped.

## 4. Numerical Procedures on the Grid

### 4.1. Velocity Components

Evolution in time of the four components of the velocity vector  $u^\alpha(t)$  of individual electrically charged particles, from  $u^\alpha(t_0)$  to  $u^\alpha(t_1)$  with  $\Delta t = t_1 - t_0$ , (with substitution of proper time  $\tau$  by the time coordinate  $t$ , involving the integration of  $u^0(\tau)$  over  $\tau$ .) according to what was discussed before, is governed by the equation of motion (20) with (22) (within appropriately small intervals of space and time coordinates). The same holds for a plasma velocity field, in which, according to the dispersion-free fluid model used here, individual particles represent co-moving fluid elements,

$$\begin{aligned} u^\alpha(\tau_1) - u^\alpha(\tau_0) &= u^\alpha(t_1) - u^\alpha(t_0) = \int_{t_0}^{t_1} \frac{du^\alpha(t)}{dt} dt \\ &= \int_{t_0}^{t_1} \left( \partial_t + v_j(t, \mathbf{x}) \partial^j \right) u^\alpha(t, \mathbf{x}) dt. \end{aligned} \quad (35)$$

The first term in the last integral of (35) refers to the *explicit* time dependence of the velocity field, (i.e. the change with time at a fixed point  $\mathbf{x}$  in space), whereas the second term describes its *implicit* time dependence, (i.e. the additional change with time of a co-moving particular fluid element.)

Here we are interested in the change with time of the velocity field at a fixed point  $\mathbf{x}$  in configuration space. Because of the given initial condition  $u^\alpha(\tau_0 = 0) \equiv u^\alpha(t_0, \mathbf{x})$  in each iteration step (where  $u^\alpha(t, \mathbf{x})$  denotes the velocity at a given point in configuration space) it follows:

$$u^\alpha(t_1, \mathbf{x}) = u^\alpha(t_1) - \int_{t_0}^{t_1} v_j(t, \mathbf{x}) \partial^j u^\alpha(t, \mathbf{x}) dt. \quad (36)$$

These are interpreting solutions of the plasma velocity field equations (24). Velocity components are required on grid points of a spherical grid, where the components of the electric field vector are suggested to be known from electric charge density averaged over each individual cell.

The integral in (36) can be evaluated in a first order scheme in time|| with  $v := -(t_1 - t) \Rightarrow \partial_t v = 1$ ,

$$\begin{aligned} u^\alpha(t_1, \mathbf{x}) &= u^\alpha(t_1) - (t_1 - t_0) v_j(t_0, \mathbf{x}) \partial^j u^\alpha(t_0, \mathbf{x}) \\ &\quad - \int_{t_0}^{t_1} (t_1 - t) \partial_t [v_j(t, \mathbf{x}) \partial^j u^\alpha(t, \mathbf{x})] dt \end{aligned} \quad (37)$$

by neglecting the integral in this evaluation. Differentiation with respect to spatial coordinates is performed numerically in a second order centered difference scheme (boundaries are treated separately, also in second order). The numerical scheme results in

$$\begin{aligned} u^\alpha(t_1, \mathbf{x}_i) &= u^\alpha(t_1) - \\ &\quad \frac{\Delta t}{\gamma} \left( v_{r,i} \frac{1}{\Delta r} + v_{\vartheta,i} \frac{1}{r \Delta \vartheta} + v_{\varphi,i} \frac{1}{r \sin \vartheta \Delta \varphi} \right) \frac{1}{2} [u^\alpha(t_0, \mathbf{x}_{i+1}) - u^\alpha(t_0, \mathbf{x}_{i-1})], \end{aligned} \quad (38)$$

|| This, of course, requests for reasonably small time steps for numerical integration.

where the index  $i$  now characterizes the  $i^{th}$  grid point (e.g. with respect to  $\mathbf{e}_r$ –direction, etc.).

#### 4.2. Electromagnetic Field Components

Numerical integration of electromagnetic field equations is performed applying a scheme developed in our group by [34], implying a (complete and orthonormal) system of spherical vector harmonics  $\mathbf{P}_{nm}$ ,  $\mathbf{B}_{nm}$ ,  $\mathbf{C}_{nm}$  (e.g. [35]),

$$\begin{aligned}\mathbf{P}_{nm}(\vartheta, \varphi) &= \mathbf{e}_r X_{nm}, \\ \mathbf{B}_{nm}(\vartheta, \varphi) &= [\mathbf{e}_r, \mathbf{C}_{nm}(\vartheta, \varphi)] = \frac{r}{\sqrt{n(n+1)}} (\nabla, X_{nm}), \\ \mathbf{C}_{nm}(\vartheta, \varphi) &= -[\mathbf{e}_r, \mathbf{B}_{nm}(\vartheta, \varphi)] = \frac{r}{\sqrt{n(n+1)}} [\nabla, \mathbf{r} X_{nm}],\end{aligned}\quad (39)$$

where  $n \in \{0, 1, 2, \dots\}$ ,  $m \in \{-n, \dots, 0, \dots, n\}$  and the spherical harmonics  $X_{nm}(\vartheta, \varphi)$  are defined with the help of the associated Legendre–function  $P_l^m(\cos \vartheta)$ ,

$$X_{nm}(\vartheta, \varphi) = e^{im\varphi} P_n^m(\cos \vartheta), \quad (40)$$

permitting the expansion of the electromagnetic vector potential,

$$\begin{aligned}\mathbf{A}(r, \vartheta, \varphi, t) &= \sum_{n,m} [p_{nm}(r, t) \mathbf{P}_{nm}(\vartheta, \varphi) \\ &\quad + b_{nm}(r, t) \mathbf{B}_{nm}(\vartheta, \varphi) + c_{nm}(r, t) \mathbf{C}_{nm}(\vartheta, \varphi)].\end{aligned}\quad (41)$$

For example, the vector potential of the Deutsch–field can be represented in the form

$$\begin{aligned}\mathbf{A}(r, \vartheta, \varphi) &= t \frac{r_N^2}{r^4} \cos \chi \mathbf{P}_{20} - ie^{-it} \frac{h_2(r)}{H_2(r_N)} \sin \chi \mathbf{P}_{21} \\ &\quad + t \frac{r_N^2}{r^4} \cos \chi \mathbf{B}_{20} - ie^{-it} \frac{H_2(r)}{r^2 H_2(r_N)} \sin \chi \mathbf{B}_{21} \\ &\quad + \frac{1}{r^2} \cos \chi \mathbf{C}_{10} + e^{-it} \frac{h_1(r)}{r_N^2 h_1(r_N)} \sin \chi \mathbf{C}_{11},\end{aligned}\quad (42)$$

with  $h_1(r) = -e^{ir \frac{(1+i/r)}{r}}$ ,  $h_2(r) = i e^{ir \frac{(1+3i/r^2-3/r^2)}{r^2}}$ ,  $H_2(r) = e^{ir \frac{(6r-r^3)+i(6-3r^2)}{r^2}}$ .

From there, the magnetic field vector is evaluated from  $\mathbf{B} = [\nabla, \mathbf{A}]$ . Exploiting the gauge invariance of the four component vector potential to eliminate  $A^0$ , the electric field vector is evaluated through  $\mathbf{E} = -\partial_t \mathbf{A}$ .

To evaluate the total electromagnetic field in terms of its expansion coefficients, we shall add the expansion coefficients of the Deutsch (vacuum) field to the expansion coefficients of the plasma field ¶. The electric (scalar) potential  $A_0(r, \psi, \alpha)$  is determined from the charge density  $\varrho(r, \vartheta, \varphi)$ ,  $A_0(\mathbf{r}) = \int \frac{\varrho(\mathbf{r}')}{|\mathbf{r}-\mathbf{r}'|} d^3 r'$ , assuming  $A_0(r_N) = A_0(\infty)$ . Furthermore,

$$\frac{1}{|\mathbf{r}-\mathbf{r}'|} = \sum_{n,m} w_{nm} \frac{r_{<}^n}{r_{>}^{n+1}} X_{nm}^*(\vartheta', \varphi') X_{nm}(\vartheta, \varphi), \quad (43)$$

¶ It should be noted that different gauges are used for the two components.

where  $w_{nm} = (n - m)!/(n + m)!$  and, by definition,  $r_<$  ( $r_>$ ) refers to the lower (upper) limit of the considered range of  $|\mathbf{r}|$  and  $|\mathbf{r}'|$ , respectively, so that

$$\begin{aligned} A_0(\mathbf{r}) &= \sum_{n,m} X_{nm}(\vartheta, \varphi) \int w_{nm} \frac{r_{<}^n}{r_{>}^{n+1}} \varrho(\mathbf{r}') X_{nm}^*(\vartheta', \varphi') d^3 r' \\ &= \sum_{n,m} x_{nm}(r) X_{nm}(\vartheta, \varphi) \end{aligned} \quad (44)$$

with

$$x_{nm}(r) = \int w_{nm} \frac{r_{<}^n}{r_{>}^{n+1}} \varrho(\mathbf{r}') X_{nm}^*(\vartheta', \varphi') d^3 r' = \int \frac{r_{<}^n}{r_{>}^{n+1}} \varrho_{nm}(r') r'^2 dr'. \quad (45)$$

Here,

$$\varrho_{nm}(r') = \int \int w_{nm} \varrho(\mathbf{r}') X_{nm}^*(\vartheta', \varphi') \sin(\vartheta') d\vartheta' d\varphi' \quad (46)$$

are the expansion coefficients of charge density.

For a thin spherical shell of thickness  $\Delta r$  these expansion coefficients are

$$x_{nm}(r) \approx \sum_j \Delta r r_j^2 \frac{r_{<}^n}{r_{>}^{n+1}} \varrho_{nm}(r_j) = \sum_j \frac{r_{<}^n}{r_{>}^{n+1}} q_{nm}(r_j) \quad (47)$$

with  $q_{nm}(r_j) = \Delta r r_j^2 \varrho_{nm}(r_j)$ .

The modes of image charges can be seen as additional modes of the surface charge density. The image charge at position  $\mathbf{r}_1$  is characterized by  $r_{sp} = r_N^2/r_1$  and  $Q(r_{sp}) = -(r_N/r_1)Q(r_1)$ . Generally,  $\mathbf{r}_{sp} = \mathbf{r}_<$  so that

$$q_{nm}(r_{sp}) = -\frac{r_N}{r_1} q_{nm}(r_1), \quad x_{nm}(r_{sp}) = \frac{r_N^n}{r_1^{n+1}} \bar{q}_{nm}(r_N), \quad (48)$$

with  $\bar{q}_{nm}(r_N) = -\frac{r_N^n}{r_1^{n+1}} q_{nm}(r_1)$ .

The total potential at grid points  $\mathbf{r} = (r_i, \vartheta_j, \varphi_k)$  inside the spherical volume is written

$$\mathcal{A}_{nm}(r_i) = \sum_{j < i} r_j^n q_{nm}(r_j), \quad (49)$$

and at grid points outside the spherical volume,

$$\mathcal{B}_{nm}(r_i) = \sum_{j > i} \frac{1}{r_j^{n+1}} q_{nm}(r_j). \quad (50)$$

From that, the potential is

$$A_0(r_i, \vartheta_j, \varphi_k) = \sum_{n,m} \mathcal{D}_{nm}(r_i) X_{nm}(\vartheta_j, \varphi_k),$$

with  $\mathcal{D}_{nm} = \mathcal{A}_{nm} r_i^{-(n+1)} + \mathcal{B}_{nm}(r_i) r_i^n$ , resulting in the coefficients of the electric field

$$\begin{aligned} p_{mn}(r) &= -\partial_r \mathcal{D}_{nm}(r), \\ b_{mn}(r) &= -\frac{\sqrt{n(n+1)}}{r} \mathcal{D}_{nm}(r), \\ c_{mn}(r) &= 0. \end{aligned} \quad (51)$$

#### 4.3. Continuity Equation

In order to integrate the continuity equation  $\partial_\mu j^\mu = 0$  the method of *flux corrected transport* (FCT) is used. This method bases on algorithmens developped by [36, 37, 38]. In a first step, a numerical ('low-order') scheme is applied providing for sufficient local numerical diffusion so that the numerical integration of the transport equation results stable and monotonous. In a second step numerical diffusion is eliminated as far as possible. When applying this concept, the effect of numerical diffusion is estimated by comparing the low-order scheme with a high-order scheme, which includes low numerical diffusion and is not monotonous. For details we refer to [38]. In the present case, this procedure has to be extended to three dimensions, which is shown in Appendix A. The result is a stable conservative discretisation scheme with low numerical diffusion.

#### 4.4. Particle Injection

Of the three frequently discussed injection mechanisms, (1) emission from the spherical surface, (as determined by the electric field topography at the surface and surface charge density,) (2) invasion of particles from outer regions, and (3) electron–positron pair creation from photon decay, we need to consider only (1) here. The rate of particle injection from the surface is chosen proportional to the magnitude of the electric field component projected onto the tangent to the corresponding magnetic field line,  $E_{||} = \text{sign}(\cos \psi)(\mathbf{E}, \mathbf{B})/B$ , if the sign of surface charge density agrees with the sign of  $E_{||}$  at the respective point on the surface.

#### 4.5. Reproducing the Magnetospheric Configuration

All simulations are started from the vacuum case. For  $\chi = 0$  ( $\chi = \pi$ ) the electric field in vacuum allows emission of electrons (protons) only, while emission regions of electrons and protons are equally large for  $\chi = \frac{\pi}{2}$ . For  $0 < \chi < \frac{\pi}{2}$  it is the emission of electrons and for  $\frac{\pi}{2} < \chi < \pi$  it is the emission of protons that predominates.

We study the magnetosphere of an initially non-charged, homogenous magnetized sphere up to  $20 r_N$  with the standard set of parameters. The following grid sizes are used in the numerical simulation:

$$\Delta t' = 5.0 \cdot 10^{-5} \text{ if } \chi = 0, \chi = \pi$$

$$\Delta t' = 2.5 \cdot 10^{-5} \text{ if } 0 < \chi < \pi$$

$$\Delta r' = 3.99 \cdot 10^{-4}$$

$$\Delta \vartheta' = \Delta \varphi' = 2.06 \cdot 10^{-4} \text{ ib}$$

$$\Delta \vartheta' = \Delta \varphi' = 4.12 \cdot 10^{-3} \text{ ob},$$

where *ib* destigates the inner border and *ob* the outer border. This resolution implies that e.g. for the (anti)parallel rotator a fluid element can cross the radial simulation extension 50 times during simulation time, which corresponds to a  $114.6^\circ$  rotation of the

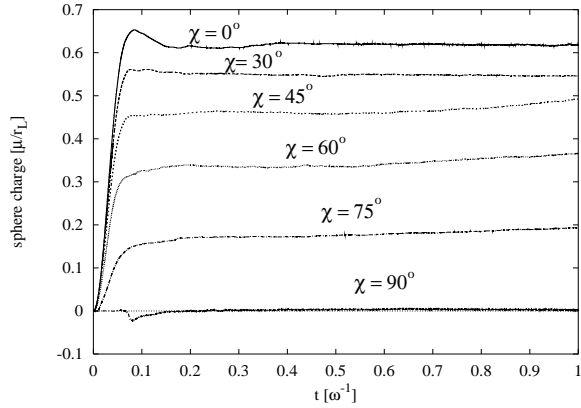


**Figure 4.** Sphere charge depending on the time for different inclination angle.

sphere. For the oblique rotator, the simulation time corresponds to a rotation of  $57.3^\circ$ , so that a fluid element can cross the radial simulation extension 25 times. Consequently, the simulation time is large enough to reproduce eventually existing quasi-stationary magnetospheres.

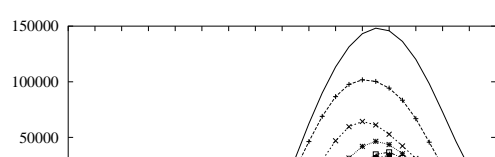
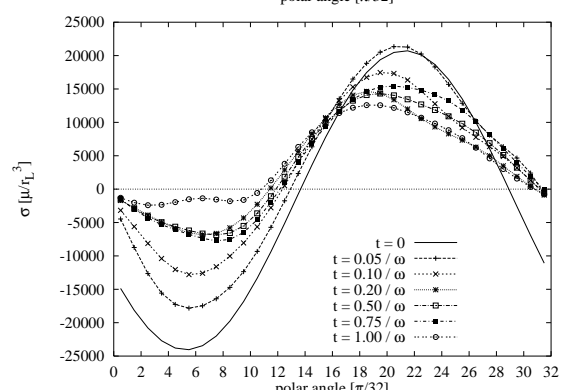
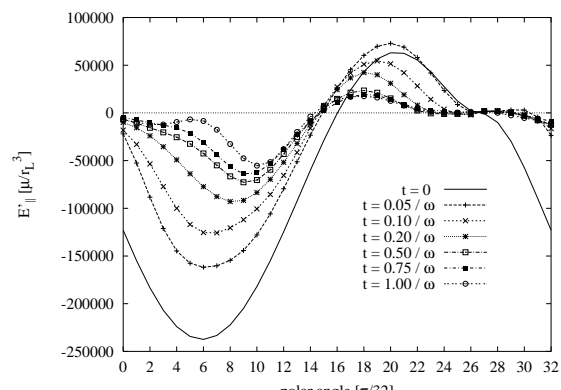
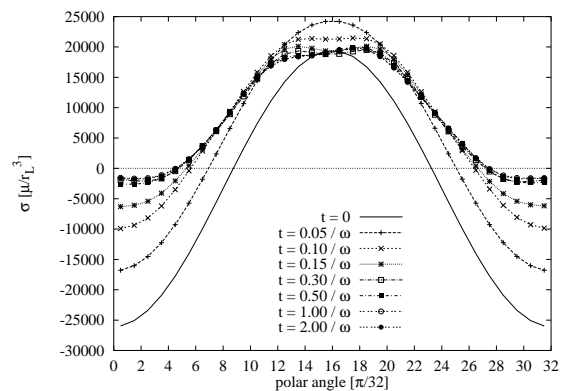
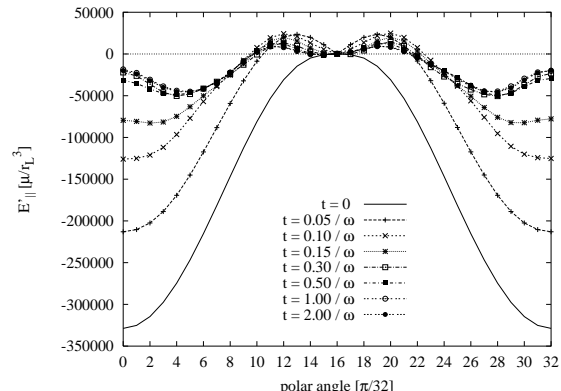
We study the rotator exemplary for several inclination angles:  $\chi = 0^\circ, 60^\circ, 90^\circ$  and – in the context of maximal particle energies –  $\chi = 120^\circ$ . Moreover, we consider  $\chi = 30^\circ, 45^\circ$  and  $\chi = 75^\circ$  in order to show the dependence from the inclination angle in detail.

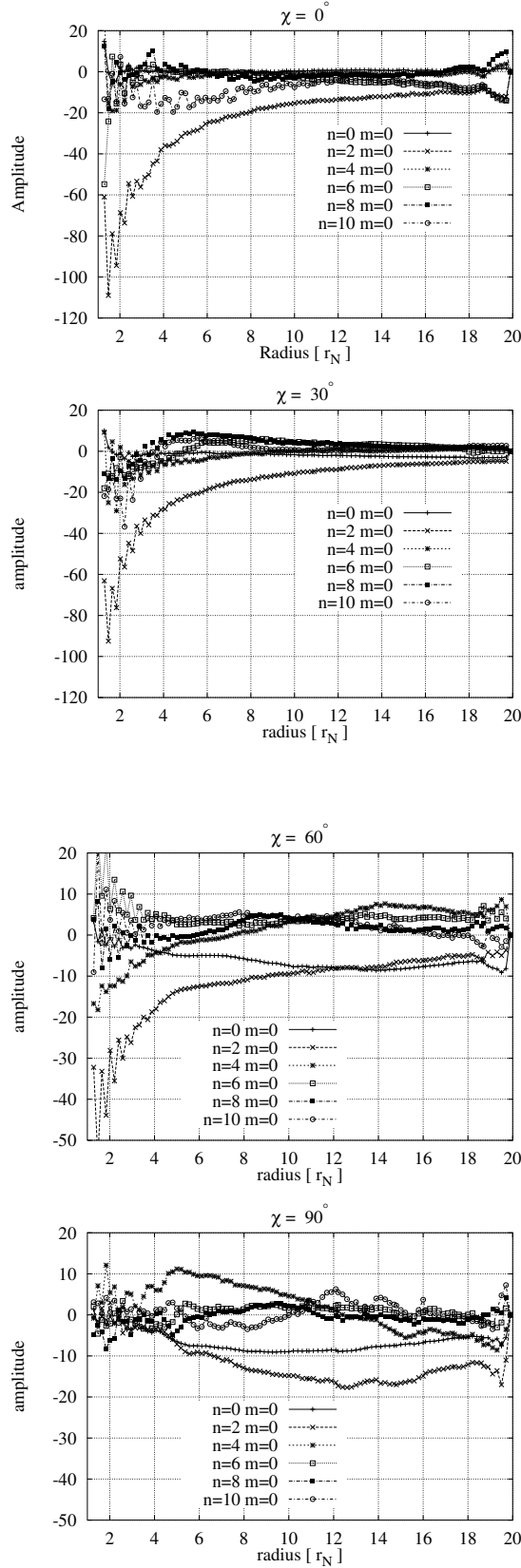
## 5. Results and Discussion

We shall present and discuss our results under the aspect of the following questions: is it possible to conclude on the formation of a (quasi-)stationary magnetosphere and if so, what can be said about some of its structural features, can predictions of the Goldreich & Julian–model and other authors in the special case of the aligned rotator be verified and what are the magnetospheric structures in the case of the inclined and orthogonal rotators, for which is little known in the published literature, and, last not least, what are the typical particle number densities and average particle energies inside that magnetospheres.

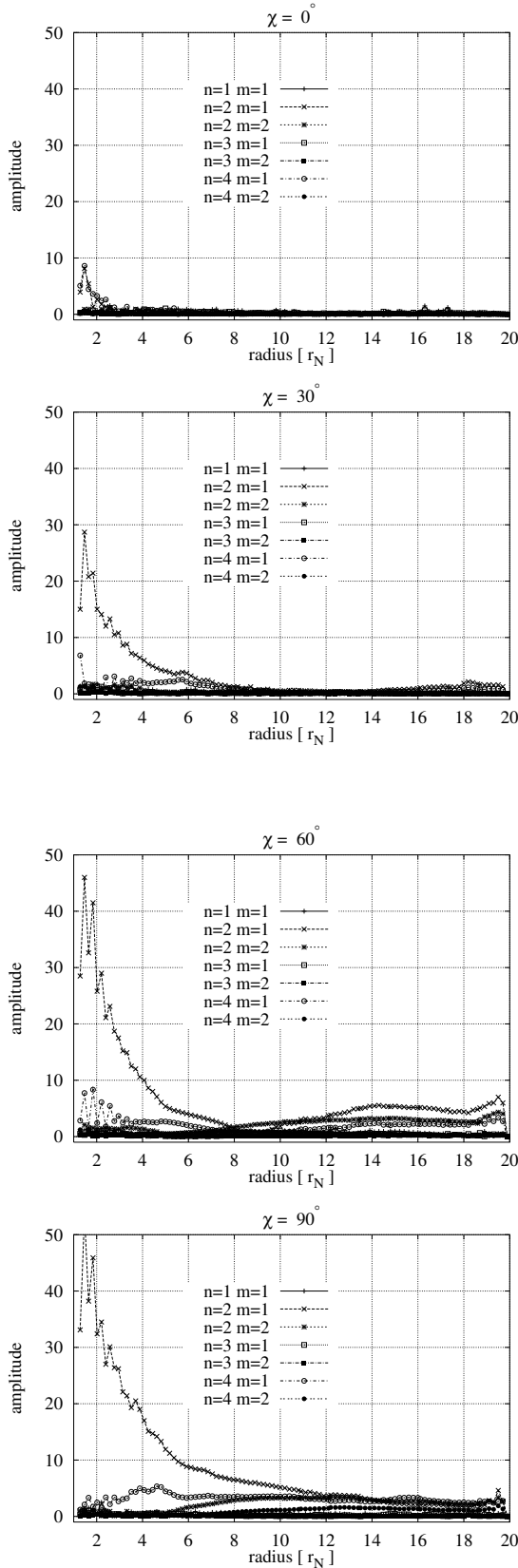
Fig. 4 demonstrates the development in time of the total electric charge of the sphere for various values of the angle of inclination  $\chi$  of the magnetic against the rotational axis, ranging from  $\chi = 0$  (top) to  $\chi = \pi/2$  (bottom). Obviously, an asymptotic value is reached in each of these cases within time intervals well below  $t \approx 0.2 \omega^{-1}$ , corresponding to a rotation of  $\approx 11.2^\circ$ . This behaviour can already be seen as a clear indication for the rapid formation of (quasi-)stationary magnetospheric configurations for all inclination angles.

Likewise, diagramms on the left of fig. 5 show the development in time of the electric vector component parallel to the tangent to the respective magnetic field line, on the stellar surface. Different curves, plotted against the polar angle, correspond to different

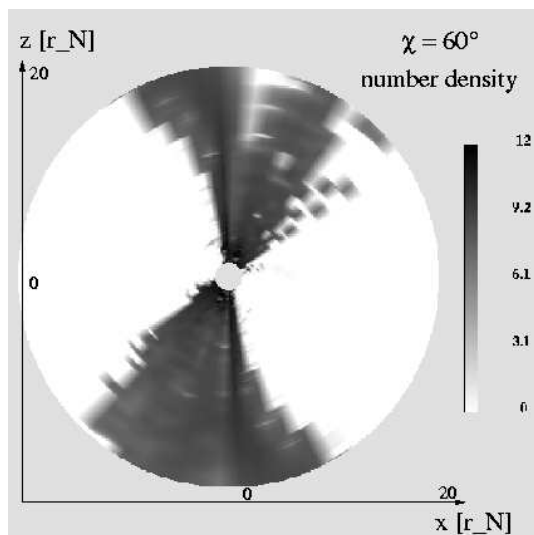
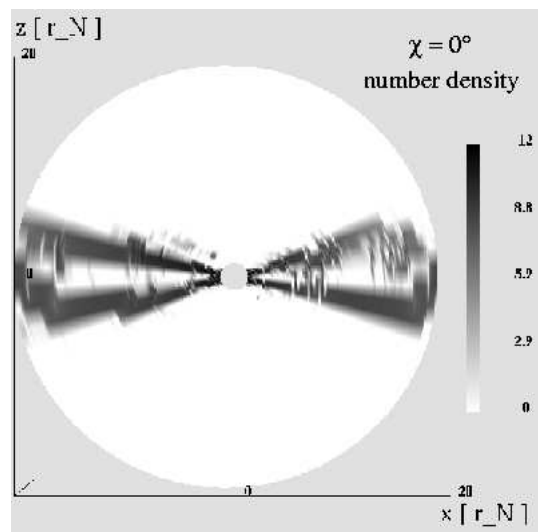
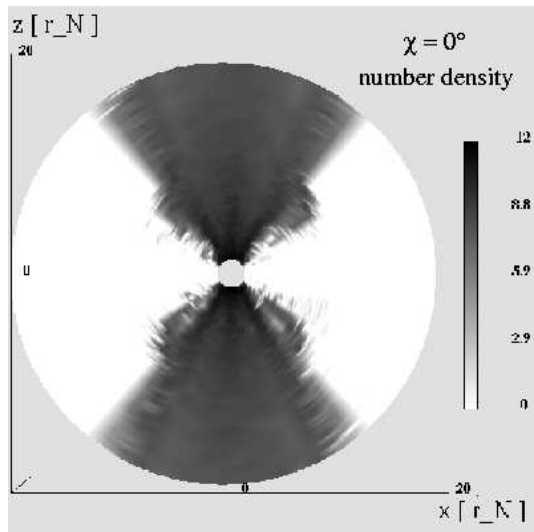


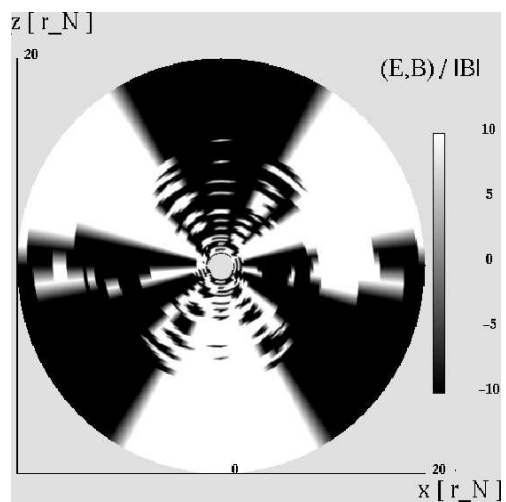
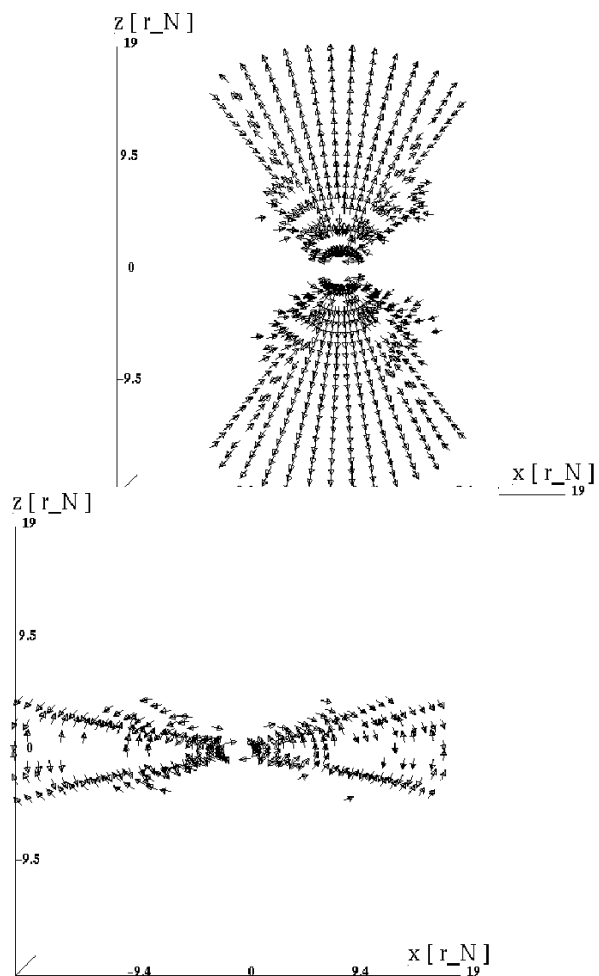


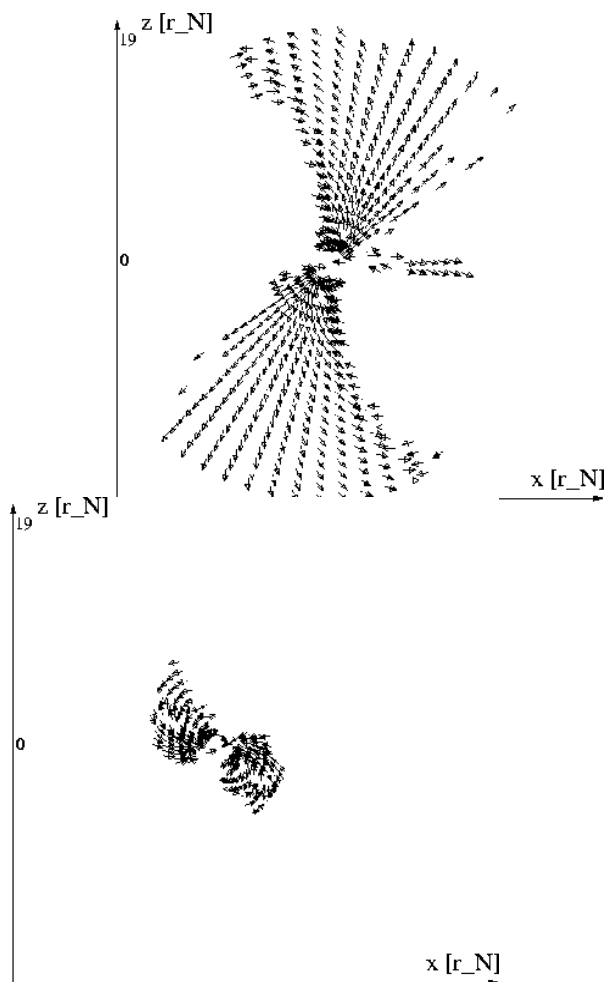
**Figure 6.** Coefficients of the charge density with  $m = 0$  in the quasi-stationary case for different inclination angles.

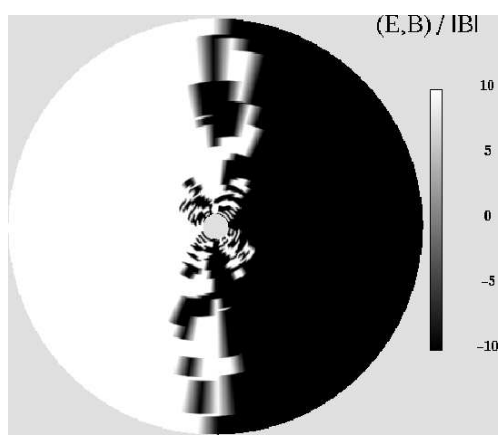
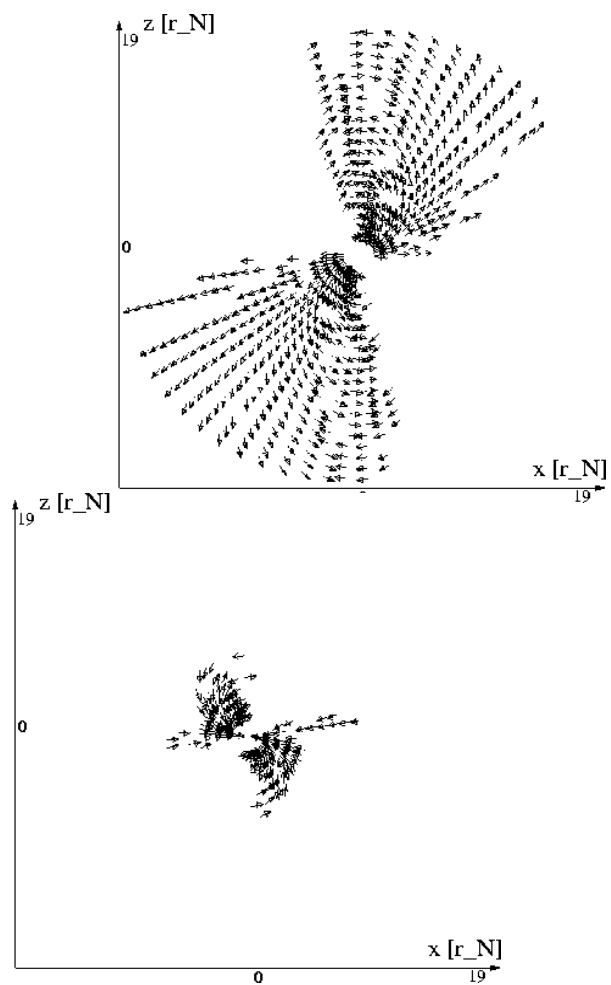


**Figure 7.** Coefficients of the space charge density with  $m \neq 0$  in the quasi-stationary case for different inclination angles.









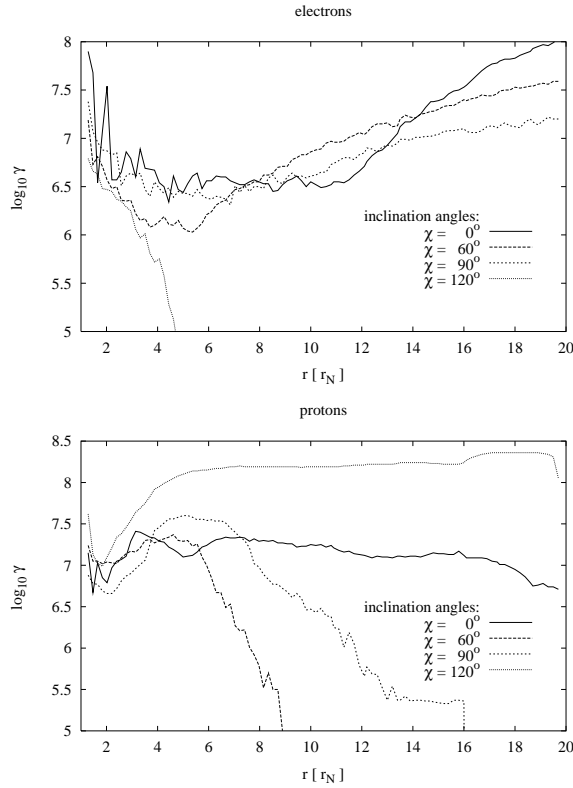


**Figure 12.** Averaged Lorentz-factors per radial sphere depending on the radius for different inclination angles.

values of the time coordinate. The three diagramms from the top to the bottom of fig. 5 are for different values of the angle of inclination ranging from  $\chi = 0^\circ$ ,  $\chi = 60^\circ$  to  $\chi = 90^\circ$ . In all of these cases, the abscissa is rapidly approached for all inclination angles, within a time interval of about  $t \approx 0.2 \omega^{-1}$ , so that again the formation of quasi stable magnetospheres is suggested.

Analogous conclusions can be drawn from diagramms on the right of fig. 5 for the elctric charge density on the surface of the sphere.

For an analysis of spatial electric charge density inside that quasi stationary magnetospheric particle distributions one may view the corresponding even modes (normalized to  $r^2$ ) in terms of coefficients of charge density (see chapter 4.2) as a function of the radial coordinate as shown in fig. 6. Different curves are for different modes, while different diagramms are for different inclination angles. In the special case of the aligned rotator, the space charge density is described fairly well only by the quadropol mode,  $n = 2, m = 0$ , in agreement with the predictions of the Goldreich & Julian-model<sup>+</sup> as well as of the more recent work by [24], while for increasing inclination angle  $\chi$ , other modes gain more and more importance, especially those with  $m \neq 0$ , responsible for

<sup>+</sup> In [6] a force-free magnetosphere ( $(\mathbf{E}, \mathbf{B}) = 0$ ) and a co-rotating plasma inside the light-cylinder are assumed. With  $\mathbf{E} = -[\beta^{\text{koro}}, \mathbf{B}]$  and  $\beta^{\text{koro}} = (r/r_L) \sin \vartheta \mathbf{e}_\varphi$ , the electric field outside the sphere results

non-axially symmetric constibutions, as shown in fig. 7.

For a better vizualization of spatial electric charge distribution inside the quasi stationary configuration, we are showing in fig. 8 distributions of electron (on the left) and proton (on the right) number densities [ $\text{cm}^{-3}$ ] within the plane spanned by the magnetic and the rotational axes ((x,z)-plane of the  $\omega$ -system ( $\lambda = 0$ )), for different angles of inclination. These pictures demonstrate the existence of completely charge seperated particle clouds devided by regions of vanishing particle number density, often refer as 'vacuum gaps'. For the inclined rotator the electrons and protons are found near the plane defined by the rotational and magnetic axis, which means a co-rotational space charge distribution in the near of the surface of the sphere up to  $\approx 10 r_N$ . Particle number densities inside these clouds, for the standard set of parameters, typically range up to  $10^{12} \text{ cm}^{-3}$ .

For a discussion on particle motion and acceleration within these clouds, normalized velocity fields of electrons (left) and protons (right) are reproduced at the two pictures at the top of fig. 9–11, and the distribution of the projection of the electric vector onto the tangent to the magnetic field lines, ( $\mathbf{E}, \mathbf{B}/|\mathbf{B}|$ ), is demonstrated by the two the pictures at the bottom in each of these figures. As can be seen, the direction of the velocity field correlates monotonously with the sign of that projection of the electric vector. In the special case of the parallel rotator, particles near the rotational axis give rise to an outward particle flux in agreement with the predictions by Goldreich & Julian (1969). Additionally, a small outward particle current created by diffusion inside the equatorial plane is formed. In the more general case of inclinded rotators, under the influence of asymmetric electric space charge configurations, outward particle currents exist, which are not so easily interpreted. Still, since particle currents extend to regions outside our simulation volume, we cannot from there comment on [7, 8] predictions of closed current systems.

Also we have studied the avaraged Lorentz–factors for electrons (left) and protons (right) in fig. 12. Average values are for spherical shells, the radius of which is given on the abscissa. Different curves are for different values of the inclination angle. For example avarage particle energies range up to  $10^{17} \text{ eV}$  for protons inside the clouds of an inclined rotator with  $\chi = 120^\circ$ . Individual particle energies, clearly, may extend to much higher values and, possible, contribute to high energy cosmic radiation, but, obviously, in:

$$\mathbf{E} = -\frac{\mu k^3}{(kr)^2} (-\sin^2 \vartheta \mathbf{e}_r + 2 \cos \vartheta \sin \vartheta \mathbf{e}_\vartheta). \quad (52)$$

This field is caused by the charge density

$$\varrho_{\text{GJ}} = -\frac{\mu}{\pi r_L} \frac{1}{r^3} P_2(\cos \vartheta) \quad (53)$$

and an additional sphere–monopol by  $q_s = \frac{2}{3} \frac{\mu}{r_L}$ . The electric potential is given by:

$$A_0 = A_0^{\text{mono}} + A_0^{\text{quadrupole}} = \frac{2}{3} \frac{\mu}{r_L} \frac{1}{r} (1 - P_2(\cos \vartheta)). \quad (54)$$

cannot be concluded upon in a statistical description, like the one applied here, with restriction to the inner part of the relativistic magnetosphere of rotating spheres.

The high particle energies in the existing poloidal currents are relevant for induced pair production. In the present paper we were able to ignore the resulting  $e^\pm$ -plasma. Nevertheless, the relativistic current in these plasmas may cause microscopic instabilities, which could explain the non-thermal radiation in such magnetospheres. Analytical studies on this topic (e.g. [39]) assume Lorentz-factors in the current of  $\gamma \approx 10^7$  and particle densities in the scale of the Goldreich & Julian-density, as were confirmed by our studies.

## Appendix A. Integration of the Continuity Equation

This appendix describes the numerical integration of the continuity equation  $\partial_\mu j^\mu = 0$  in detail. The used method is called *flux corrected transport* (FCT), and for details regarding general aspects of this method we refer to [38].

In the following we introduce a 'low-order' and a 'high-order' scheme in three spatial coordinates in order to construct a conservative FCT scheme. A spherical coordinate system is used, and  $i, j, k$  denote the grid points in the  $\mathbf{e}_r, \mathbf{e}_\theta$  and  $\mathbf{e}_\varphi$ -direction.

The flux which flows from the cell  $i-1$  to cell  $i$  is called  $F_{i-\frac{1}{2},j,k}$  and the flux from cell  $i$  to cell  $i+1$   $F_{i+\frac{1}{2},j,k}$ .  $G$  and  $H$  are the corresponding fluxes in  $\mathbf{e}_\theta$ - and  $\mathbf{e}_\varphi$ -direction. With this notation a conservative discretisation is given by:

$$\varrho_{i,j,k}^{n+1} = \varrho_{i,j,k}^n - F_{i+\frac{1}{2},j,k} + F_{i-\frac{1}{2},j,k} - G_{i,j+\frac{1}{2},k} + G_{i,j-\frac{1}{2},k} - H_{i,j,k+\frac{1}{2}} + H_{i,j,k-\frac{1}{2}}. \quad (\text{A.1})$$

As the 'low-order' scheme we use the Donor-Cell method in three dimensions

$$\begin{aligned} \varrho_{i,j,k}^{n+1} = & \varrho_{i,j,k}^n - 0.5(\xi_1 - |\xi_1|) \varrho_{i+1,j,k}^n + 0.5(\xi_1 + |\xi_1|) \varrho_{i-1,j,k}^n \\ & - 0.5(\xi_2 - |\xi_2|) \varrho_{i,j+1,k}^n + 0.5(\xi_2 + |\xi_2|) \varrho_{i,j-1,k}^n \\ & - 0.5(\xi_3 - |\xi_3|) \varrho_{i,j,k+1}^n + 0.5(\xi_3 + |\xi_3|) \varrho_{i,j,k-1}^n, \end{aligned} \quad (\text{A.2})$$

with the Courant-numbers  $\xi$  concerning the three spatial coordinates which are indicated by the indices 1, 2, 3. The stability condition regarding this 'low-order' scheme is given by:

$$|\xi_1| + |\xi_2| + |\xi_3| \leq 1. \quad (\text{A.3})$$

A stable 'high-order' scheme (in three spatial coordinates) is developed by [40]:

$$\varrho^{n+1} = \varrho^n - \Delta t (\nabla, (\varrho \mathbf{v} - 0.5 \Delta t \mathbf{v}(\nabla, n\mathbf{v}))). \quad (\text{A.4})$$

Now we are able to write down the discretisation schemes. In the following we use dimensionless units  $\Delta t' = \omega \Delta t$  and  $\Delta r' = r_L^{-1} \Delta r$  and suppress the primes. The continuity equation is now given by

$$\partial_t N + \partial_i N \beta^i = 0, \quad (\text{A.5})$$

where  $N$  is the particle density in the inertial frame of reference.

The currents regarding the Donor-Cell method are given by

$$(N \beta_r)_{i+\frac{1}{2},j,k} = \frac{1}{2} [(\beta_r)_{i+1,j,k} - |(\beta_r)_{i+1,j,k}|) N_{i+1,j,k} \quad (A.6)$$

$$+ \frac{1}{2} ((\beta_r)_{i,j,k} + |(\beta_r)_{i,j,k}|) N_{i,j,k} ,$$

$$(N \beta_\vartheta)_{i,j+\frac{1}{2},k} = \frac{1}{2} [(\beta_\vartheta)_{i,j+1,k} - |(\beta_\vartheta)_{i,j+1,k}|) N_{i,j+1,k} \quad (A.7)$$

$$+ \frac{1}{2} ((\beta_\vartheta)_{i,j,k} + |(\beta_\vartheta)_{i,j,k}|) N_{i,j,k} ,$$

$$(N \beta_\varphi)_{i,j,k+\frac{1}{2}} = \frac{1}{2} [(\beta_\varphi)_{i,j,k+1} - |(\beta_\varphi)_{i,j,k+1}|) N_{i,j,k+1} \quad (A.8)$$

$$+ \frac{1}{2} ((\beta_\varphi)_{i,j,k} + |(\beta_\varphi)_{i,j,k}|) N_{i,j,k} .$$

With the following abbreviations for the surface elements

$$\text{Fl}_{r,(i,j,k)} = 2 r_i^2 \sin \vartheta_j \sin \frac{\Delta \vartheta_j}{2} \Delta \varphi_k ,$$

$$\text{Fl}_{\vartheta,(i,j,k)} = \frac{1}{2} (r_{i+\frac{1}{2}}^2 - r_{i-\frac{1}{2}}^2) \sin \vartheta_j \Delta \varphi_k ,$$

$$\text{Fl}_{\varphi,(i,j,k)} = \frac{1}{2} (r_{i+\frac{1}{2}}^2 - r_{i-\frac{1}{2}}^2) \Delta \vartheta_j$$

the fluxes result in

$$\begin{aligned} F_{i+\frac{1}{2},j,k} &= \Delta t \text{Fl}_{r,(i+\frac{1}{2},j,k)} [ \min(0, (\beta_r)_{i+1,j,k}) N_{i+1,j,k} \\ &\quad + \max(0, (\beta_r)_{i,j,k}) N_{i,j,k} ] , \\ G_{i,j+\frac{1}{2},k} &= \Delta t \text{Fl}_{\vartheta,(i,j+\frac{1}{2},k)} [ \min(0, (\beta_\vartheta)_{i,j+1,k}) N_{i,j+1,k} \quad (A.9) \\ &\quad + \max(0, (\beta_\vartheta)_{i,j,k}) N_{i,j,k} ] , \\ H_{i,j,k+\frac{1}{2}} &= \Delta t \text{Fl}_{\varphi,(i,j,k+\frac{1}{2})} [ \min(0, (\beta_\varphi)_{i,j,k+1}) N_{i,j,k+1} \\ &\quad + \max(0, (\beta_\varphi)_{i,j,k}) N_{i,j,k} ] . \end{aligned}$$

With the fluxes (A.9) the 'low-order' scheme is given by

$$\begin{aligned} N_{i,j,k}^{n+1} &= N_{i,j,k}^n + \frac{1}{\Delta V_{i,j,k}} [ -F_{i+\frac{1}{2},j,k} + F_{i-\frac{1}{2},j,k} \\ &\quad -G_{i,j+\frac{1}{2},k} + G_{i,j-\frac{1}{2},k} - H_{i,j,k+\frac{1}{2}} + H_{i,j,k-\frac{1}{2}} ] . \end{aligned} \quad (A.10)$$

Referring to (A.4) the 'high-order' scheme is given by

$$\begin{aligned} N^{n+1} &= N^n - \Delta t \left[ \frac{1}{r^2} \partial_r \left( r^2 \left( N \beta_r - \frac{1}{2} \Delta t \beta_r g \right) \right) \right. \\ &\quad + \frac{1}{r \sin \vartheta} \partial_\vartheta \left( \sin \vartheta \left( N \beta_\vartheta - \frac{1}{2} \Delta t \beta_\vartheta g \right) \right) \\ &\quad \left. + \frac{1}{r \sin \vartheta} \partial_\varphi \left( N \beta_\varphi - \frac{1}{2} \Delta t \beta_\varphi g \right) \right] , \end{aligned} \quad (A.11)$$

with

$$\begin{aligned} g := \partial_i(N \beta^i) &= \frac{1}{r^2} \partial_r (r^2 N \beta_r) + \frac{1}{r \sin \vartheta} \partial_\vartheta (\sin \vartheta N \beta_\vartheta) \\ &\quad + \frac{1}{r \sin \vartheta} \partial_\varphi (N \beta_\varphi) . \end{aligned} \quad (A.12)$$

The fluxes regarding the 'high-order' scheme result in:

$$F_{i+\frac{1}{2},j,k} = \Delta t \text{Fl}_{\varrho, (i+\frac{1}{2},j,k)} \left[ (N \beta_r)_{i+\frac{1}{2},j,k} - \frac{1}{2} \Delta t (\beta_r)_{i+\frac{1}{2},j,k} \left[ \begin{array}{l} \frac{1}{r_{i+\frac{1}{2}}^2 \Delta r} \left( (r^2 N \beta_r)_{i+1,j,k} - (r^2 N \beta_r)_{i,j,k} \right) \\ + \frac{1}{4 r_{i+\frac{1}{2}} \sin \vartheta_j \Delta \vartheta} \left[ \sin \vartheta_{j+1} ((N \beta_\vartheta)_{i,j+1,k} + (N \beta_\vartheta)_{i+1,j+1,k}) \right. \\ \left. - \sin \vartheta_{j-1} ((N \beta_\vartheta)_{i,j-1,k} + (N \beta_\vartheta)_{i+1,j-1,k}) \right] \\ + \frac{1}{4 r_{i+\frac{1}{2}} \sin \vartheta \Delta \varphi} \left[ (N \beta_\varphi)_{i,j,k+1} + (N \beta_\varphi)_{i+1,j,k+1} \right. \\ \left. - ((N \beta_\varphi)_{i,j,k-1} + (N \beta_\varphi)_{i+1,j,k-1}) \right] \end{array} \right] \right], \quad (\text{A.13})$$

$$G_{i,j+\frac{1}{2},k} = \Delta t \text{Fl}_{\vartheta, (i,j+\frac{1}{2},k)} \left[ (\sin \vartheta N \beta_\vartheta)_{i,j+\frac{1}{2},k} - \frac{1}{2} \Delta t (\sin \vartheta \beta_\vartheta)_{i,j+\frac{1}{2},k} \left[ \begin{array}{l} \frac{1}{r \sin \vartheta_{j+\frac{1}{2}} \Delta \vartheta} \left[ (\sin \vartheta N \beta_\vartheta)_{i,j+1,k} - (\sin \vartheta N \beta_\vartheta)_{i,j,k} \right] \\ + \frac{1}{4 r^2 \Delta r} \left[ r_{i+1}^2 ((N \beta_r)_{i+1,j,k} + (N \beta_r)_{i+1,j+1,k}) \right. \\ \left. - r_{i-1}^2 ((N \beta_r)_{i-1,j,k} + (N \beta_r)_{i-1,j+1,k}) \right] \\ + \frac{1}{4 r \sin \vartheta_{j+\frac{1}{2}} \Delta \varphi} \left[ (N \beta_\varphi)_{i,j,k+1} + (N \beta_\varphi)_{i,j+1,k+1} \right. \\ \left. - ((N \beta_\varphi)_{i,j,k-1} + (N \beta_\varphi)_{i,j+1,k-1}) \right] \end{array} \right] \right], \quad (\text{A.14})$$

$$H_{i,j,k+\frac{1}{2}} = \Delta t \text{Fl}_{\varphi, (i,j,k)} \left[ (N \beta_\varphi)_{i,j,k+\frac{1}{2}} - \frac{1}{2} \Delta t (\beta_\varphi)_{i,j,k+\frac{1}{2}} \left[ \begin{array}{l} \frac{1}{r \sin \vartheta \Delta \varphi} \left[ (N \beta_\varphi)_{i,j,k+1} - (N \beta_\varphi)_{i,j,k} \right] \\ + \frac{1}{4 r^2 \Delta r} \left[ r_{i+1}^2 ((N \beta_r)_{i+1,j,k} + (N \beta_r)_{i+1,j,k+1}) \right. \\ \left. - r_{i-1}^2 ((N \beta_r)_{i-1,j,k} + (N \beta_r)_{i-1,j,k+1}) \right] \\ + \frac{1}{4 r \sin \vartheta \Delta \vartheta} \left[ \sin \vartheta_{j+1} ((N \beta_\vartheta)_{i,j+1,k} + (N \beta_\vartheta)_{i,j+1,k+1}) \right. \\ \left. - \sin \vartheta_{j-1} ((N \beta_\vartheta)_{i,j-1,k} + (N \beta_\vartheta)_{i,j-1,k+1}) \right] \end{array} \right] \right]. \quad (\text{A.15})$$

Using the mentioned fluxes for the 'low-' and the 'high-order' scheme the construction of a full FCT scheme is straightforward (for details we refer to [38]). This FCT scheme is stable if the following conditions are fulfilled:

$$|\xi_1|^{\frac{2}{3}} + |\xi_2|^{\frac{2}{3}} + |\xi_3|^{\frac{2}{3}} \leq 1, \quad (\text{A.16})$$

$$\Delta t \leq \left[ \left( \frac{|\beta_r|}{\Delta r} \right)^{\frac{2}{3}} + \left( \frac{|\beta_\vartheta|}{r \Delta \vartheta} \right)^{\frac{2}{3}} + \left( \frac{|\beta_\varphi|}{r \sin \vartheta \Delta \varphi} \right)^{\frac{2}{3}} \right]^{-\frac{3}{2}}. \quad (\text{A.17})$$

## References

- [1] Hewish A, Bell S J, Pilkington D H, Scott P F and Collins R A 1968 *Nature (London)* **217** 709
- [2] Gold T 1968 *Nature (London)* **218** 731
- [3] Pacini F 1968 *Nature* **219** 145
- [4] Ostriker J P and Gunn J E 1969 *ApJ* **157** 1395
- [5] Gunn J E and Ostriker J P 1971 *Apj* **165** 523
- [6] Goldreich P and Julian W H 1969 *ApJ* **157** 869
- [7] Jackson A 1976 *ApJ* **206** 831
- [8] Jackson A 1978 *ApJ* **222** 675
- [9] Endean V G 1976 *MNRAS* **174** 125
- [10] Uchida T 1998 *MNRAS* **297** 315
- [11] Shibata S 1989 *Astrophys. Space Sci.* **161** 145
- [12] Mestel L, Robertson J A, Wang Y M and Westfold K C 1985 *MNRAS* **217** 443
- [13] Fitzpatrick R and Mestel L 1988a *MNRAS* **232** 277
- [14] Fitzpatrick R and Mestel L 1988b *MNRAS* **232** 303
- [15] Kaburaki O 1985a *Astrophys. Space Sci.* **112** 157
- [16] Kaburaki O 1985b *Astrophys. Space Sci.* **112** 287
- [17] Rylov Yu A 1989 *Astrophys. Space Sci.* **158.2** 297
- [18] Rylov, Yu A 1992 *Proc. of IAU Coll 128* eds. Hankins, Rankin, Gil, 98
- [19] Kuo-Petravic L G, Petravic M and Roberts K V 1974 *Phys. Rev. Letter* **32** 1019
- [20] Kuo-Petravic L G, Petravic M and Roberts K V 1975 *ApJ* **202** 762
- [21] Krause-Polsdorff J and Michel F C 1985 *Astrophys. and Astronomy* **144** 72
- [22] Ertl T 1988 *Ph. D. thesis* University Tübingen
- [23] Zachariades H A 1993 *Astrophys. and Astronomy* **268** 705
- [24] Neukirch T 1993 *Astrophys. and Astronomy* **274** 319
- [25] Thielheim K O and Wolfsteller H 1989 *ApJS* **71** 583
- [26] Thielheim K O and Wolfsteller H 1994 *ApJ* **431** 718
- [27] Laue H and Thielheim K O 1986 *ApJS* **61** 465
- [28] Thielheim K O 1991 *Nuclear Phys. (Proc. Suppl.)* **22B** 60
- [29] Thielheim K O 1994 *Physica Scripta* **T52** 123
- [30] Deutsch A J 1955 *Annales d'Astrophysique* **18** 1
- [31] Dirac P M A 1938 *Proceedings of the Royal Society London A* **167** 148
- [32] Thielheim K O 1989 *Fundamentals of Cosmic Physics* **13** 357
- [33] Landau L M and Lifshitz E M 1977 *Klassische Feldtheorie*, Akademie-Verlag Berlin
- [34] Laue H 1992 *Ph. D. thesis* University Kiel
- [35] Morse P M and Feshbach H 1969 *Methods of Theoretical Physics*, Part II, International Series in Pure and Applied Physics, McGraw-Hill Book Company, New York
- [36] Boris J P and Book D L 1973 *J. of Computational Phys.* **11** 38
- [37] Book D L, Boris J P and Hain K 1975 *J. of Computational Phys.* **18** 248
- [38] Zalesak S T 1979 *J. of Computational Phys.* **31** 335
- [39] Lyutikov M, Blandford R D and Machabeli G. 1999 *MNRAS* **305** 338
- [40] Dukowicz J K, Ramshaw J D 1979 *Journal of Computational Physics* **32** 71